Study of lepton EDMs in the $U(1)_X$ SSM*

Lu-Hao Su(苏路豪)[1,2†] Dan He(何丹)[1,2‡] Xing-Xing Dong(董幸幸)[1,2§]
Tai-Fu Feng(冯太傅)[1,2,3♮] Shu-Min Zhao(赵树民)[1,2♯]

[1]Department of Physics, Hebei University, Baoding 071002, China
[2]Key Laboratory of High-precision Computation and Application of Quantum Field Theory of Hebei Province, Baoding 071002, China
[3]Department of Physics, Chongqing University, Chongqing 401331, China

Abstract: The minimal supersymmetric extension of the standard model (MSSM) is extended to the $U(1)_X$SSM, whose local gauge group is $SU(3)_C \times SU(2)_L \times U(1)_Y \times U(1)_X$. To obtain the $U(1)_X$SSM, we add new superfields to the MSSM, namely, three Higgs singlets $\hat{\eta}$, $\hat{\bar{\eta}}$, $\hat{S}$ and right-handed neutrinos $\hat{\nu}_i$. The charge conjugate and parity (*CP*) violating effects are considered to study the lepton electric dipole moment (EDM) in the $U(1)_X$SSM. There are more *CP* violating phases in the $U(1)_X$SSM than in the standard model (SM). In this model, several new parameters $(\theta_S, \theta_{BB'}, \theta_{BL})$ are considered as *CP* violating phases; hence, there are new contributions to lepton EDMs. This is conducive to exploring the source of *CP* violation and probing new physics beyond the SM.

Keywords: lepton, electric dipole moment

DOI: 10.1088/1674-1137/ac6e35

I. INTRODUCTION

In 1964, Cronin and Fitch discovered charge conjugate and parity (*CP*) violation from the decays of the K meson [1], and lepton electric dipole moments (EDMs) have become a physical quantity used to probe sources of *CP* violation [2]. Therefore, it is important to research the EDMs of leptons. At present, the upper bound of the electron EDM is $|d_e^{\exp}| < 1.1 \times 10^{-29}$ e.cm at the 90% confidence level [3– 5], whereas that of the muon EDM is $|d_\mu^{\exp}| < 1.8 \times 10^{-19}$ e.cm at the 95% confidence level and that of the tau EDM is $|d_\tau^{\exp}| < 1.1 \times 10^{-17}$ e.cm at the 95% confidence level [6]. The sources and mechanism of *CP* violation have not been well explained, and scientists have been attempting to find *CP* violation terms in new physics beyond the SM to better explain the *CP* violation mechanism [7– 10]. There are several *CP* violating phases, which can provide large contributions to the EDMs of leptons in the minimal supersymmetric extension of the standard model (MSSM) [11–14].

Owing to the deficiency of the MSSM, which cannot explain neutrino mass or solve the μ problem, a $U(1)$ extension of the MSSM is performed. There are two $U(1)$ groups in the $U(1)_X$SSM: $U(1)_Y$ and $U(1)_X$, and the $U(1)_X$SSM is explored using SARAH software packages [15– 17]. By adding new superfields to the MSSM, the $U(1)_X$SSM not only obtains additional Higgs, neutrinos, and gauge fields, but corresponding superpartners that extend the neutralino and sfermion sectors. The mass m_{h_0} of the lightest *CP*-even Higgs [18, 19] in the $U(1)_X$SSM is larger than its corresponding mass in the MSSM at tree order. Therefore, in the $U(1)_X$SSM, the loop diagram correction of m_{h_0} does not need to be large.

An effective way to explore new physics beyond the standard model (SM) is through researching the MDMs [20, 21] and EDMs [22–28] of leptons. The one-loop and two-loop corrections to lepton EDMs have been well researched in the MSSM. d_e in the SM was studied independently of the model [29, 30], and the authors considered right-handed neutrinos, the neutrino see-saw mechanism, and the structure of minimal flavor violation. The results showed that when neutrinos are Majorana

Received 29 March 2022; Accepted 10 May 2022; Published online 1 July 2022

* Supported by National Natural Science Foundation of China (NNSFC) (11535002, 11705045), Natural Science Foundation of Hebei Province (A2020201002) and the youth top-notch talent support program of the Hebei Province

† E-mail: suluhao0606@163.com
‡ E-mail: hedandeya@163.com
§ E-mail: dxx_0304@163.com
♮ E-mail: fengtf@hbu.edu.cn
♯ E-mail: zhaosm@hbu.edu.cn

particles, the value of d_e will reach the upper limit of the experiment.

This paper is organized as follows: We introduce the specific form of the $U(1)_X$SSM and its superfields in Section II. In Section III, we show the one-loop and two-loop corrections to lepton EDMs. The main content of Section IV is a numerical analysis on the dependence of lepton EDMs on $U(1)_X$SSM parameters. We provide a summary and discussion in Section V. The appendix contains mass matrics.

II. $U(1)_X$SSM

The $U(1)_X$SSM is expanded on the basis of the MSSM. $U(1)_X$SSM superfields include three Higgs singlets $\hat{\eta}$, $\hat{\bar{\eta}}$, $\hat{S}$ and right-handed neutrinos $\hat{\nu}_i$. Via the seesaw mechanism, light neutrinos can obtain tiny masses at the tree level. For details on the mass matrices of particles, see Ref. [31].

The superpotential of the $U(1)_X$SSM is

$$W = l_W\hat{S} + \mu\hat{H}_u\hat{H}_d + M_S\hat{S}\hat{S} - Y_d\hat{d}\hat{q}\hat{H}_d - Y_e\hat{e}\hat{l}\hat{H}_d + \lambda_H\hat{S}\hat{H}_u\hat{H}_d + \lambda_C\hat{S}\hat{\eta}\hat{\bar{\eta}} + \frac{\kappa}{3}\hat{S}\hat{S}\hat{S} + Y_u\hat{u}\hat{q}\hat{H}_u + Y_X\hat{\nu}\hat{\bar{\eta}}\hat{\nu} + Y_\nu\hat{\nu}\hat{l}\hat{H}_u\,. \tag{1}$$

The two Higgs doublets and three Higgs singlets are shown below in concrete form.

$$\begin{aligned}
H_u &= \begin{pmatrix} H_u^+ \\ \frac{1}{\sqrt{2}}\left(v_u + H_u^0 + \mathrm{i}P_u^0\right) \end{pmatrix}, \\
H_d &= \begin{pmatrix} \frac{1}{\sqrt{2}}\left(v_d + H_d^0 + \mathrm{i}P_d^0\right) \\ H_d^- \end{pmatrix}, \\
\eta &= \frac{1}{\sqrt{2}}\left(v_\eta + \phi_\eta^0 + \mathrm{i}P_\eta^0\right), \\
\bar{\eta} &= \frac{1}{\sqrt{2}}\left(v_{\bar{\eta}} + \phi_{\bar{\eta}}^0 + \mathrm{i}P_{\bar{\eta}}^0\right), \\
S &= \frac{1}{\sqrt{2}}\left(v_S + \phi_S^0 + \mathrm{i}P_S^0\right).
\end{aligned} \tag{2}$$

v_u, v_d, v_η, $v_{\bar{\eta}}$, and v_S are the VEVs of the Higgs superfields H_u, H_d, η, $\bar{\eta}$, and S, respectively.

Here, we set $\tan\beta = v_u/v_d$ and $\tan\beta_\eta = v_{\bar{\eta}}/v_\eta$. The specific forms of $\tilde{\nu}_L$ and $\tilde{\nu}_R$ are

$$\tilde{\nu}_L = \frac{1}{\sqrt{2}}\phi_l + \frac{\mathrm{i}}{\sqrt{2}}\sigma_l\,, \quad \tilde{\nu}_R = \frac{1}{\sqrt{2}}\phi_R + \frac{\mathrm{i}}{\sqrt{2}}\sigma_R\,. \tag{3}$$

The specific form of soft SUSY breaking terms are shown below.

$$\begin{aligned}
\mathcal{L}_{\rm soft} =& \mathcal{L}_{\rm soft}^{\rm MSSM} - B_S S^2 - L_S S - \frac{T_\kappa}{3}S^3 - T_{\lambda_C}S\eta\bar{\eta} \\
&+ \epsilon_{ij}T_{\lambda_H}S H_d^i H_u^j - T_X^{IJ}\bar{\eta}\tilde{\nu}_R^{*I}\tilde{\nu}_R^{*J} + \epsilon_{ij}T_\nu^{IJ}H_u^i\tilde{\nu}_R^{I*}\tilde{l}_j^J \\
&- m_\eta^2|\eta|^2 - m_{\bar{\eta}}^2|\bar{\eta}|^2 - m_S^2 S^2 - (m_{\tilde{\nu}_R}^2)^{IJ}\tilde{\nu}_R^{I*}\tilde{\nu}_R^J \\
&- \frac{1}{2}\left(M_S\lambda_{\tilde{X}}^2 + 2M_{BB'}\lambda_{\tilde{B}}\lambda_{\tilde{X}}\right) + \text{h.c.}\,.
\end{aligned} \tag{4}$$

The particle content and charge assignments of the $U(1)_X$SSM are shown in Table 1. Compared to the SM, the anomalies of the $U(1)_X$SSM are more complex [32]. This model was eventually proven to be anomaly free [31]. The two Abelian groups $U(1)_Y$ and $U(1)_X$ in the $U(1)_X$SSM can create a new effect known as gauge kinetic mixing. This effect can also be induced by RGEs, even with a zero value at $M_{\rm GUT}$.

The general form of the covariant derivative of this model is [33–35]

$$D_\mu = \partial_\mu - \mathrm{i}\begin{pmatrix} Y, & X \end{pmatrix}\begin{pmatrix} g_Y, & g'_{YX} \\ g'_{XY}, & g'_X \end{pmatrix}\begin{pmatrix} A_\mu'^Y \\ A_\mu'^X \end{pmatrix}. \tag{5}$$

$A_\mu'^Y$ and $A_\mu'^X$ represent the gauge fields of $U(1)_Y$ and $U(1)_X$. Because these two Abelian gauge groups are unbroken, we perform a basis exchange. Using the orthogonal matrix R [33, 35], the resulting formula is

$$\begin{pmatrix} g_Y, & g'_{YX} \\ g'_{XY}, & g'_X \end{pmatrix}R^T = \begin{pmatrix} g_1, & g_{YX} \\ 0, & g_X \end{pmatrix}. \tag{6}$$

We deduce $\sin^2\theta_W' =$

$$\frac{1}{2} - \frac{((g_{YX}+g_X)^2-g_1^2-g_2^2)v^2+4g_X^2\xi^2}{2\sqrt{((g_{YX}+g_X)^2+g_1^2+g_2^2)^2v^4+8g_X^2((g_{YX}+g_X)^2-g_1^2-g_2^2)v^2\xi^2+16g_X^4\xi^4}}\,. \tag{7}$$

with $\xi = \sqrt{v_\eta^2 + v_{\bar{\eta}}^2}$. The new mixing angle θ_W' can be

Table 1. Superfields in the $U(1)_X$SSM.

Superfields	$SU(3)_C$	$SU(2)_L$	$U(1)_Y$	$U(1)_X$
$\hat{Q}_i$	3	2	1/6	0
$\hat{u}_i^c$	$\bar{3}$	1	−2/3	−1/2
$\hat{d}_i^c$	$\bar{3}$	1	1/3	1/2
$\hat{L}_i$	1	2	−1/2	0
$\hat{e}_i^c$	1	1	1	1/2
$\hat{\nu}_i$	1	1	0	−1/2
$\hat{H}_u$	1	2	1/2	1/2
$\hat{H}_d$	1	2	−1/2	−1/2
$\hat{\eta}$	1	1	0	−1
$\hat{\bar{\eta}}$	1	1	0	1
$\hat{S}$	1	1	0	0

found in the couplings of Z and Z'.

Next, we describe several of the required couplings.

The couplings of $\tilde{\nu}_k^R - \bar{e}_i - \chi_j^-$ and $\tilde{\nu}_k^I - \bar{e}_i - \chi_j^-$ are

$$\mathcal{L}_{\tilde{\nu}^R\bar{e}\chi^-} = \bar{e}_i\left\{\frac{\mathrm{i}}{\sqrt{2}}U_{j2}^* Z_{ki}^{R*} Y_e^i P_L - \frac{\mathrm{i}}{\sqrt{2}} g_2 V_{j1} Z_{ki}^{R*} P_R\right\}\chi_j^- \tilde{\nu}_k^R, \quad (8)$$

$$\mathcal{L}_{\tilde{\nu}^I\bar{e}\chi^-} = \bar{e}_i\left\{\frac{-1}{\sqrt{2}}U_{j2}^* Z_{ki}^{I*} Y_e^i P_L + \frac{1}{\sqrt{2}} g_2 V_{j1} Z_{ki}^{I*} P_R\right\}\chi_j^- \tilde{\nu}_k^I. \quad (9)$$

With $P_L = \frac{1-\gamma_5}{2}$ and $P_R = \frac{1+\gamma_5}{2}$. Z^R and Z^I are rotation matrices, which can diagonalize the mass squared matrices of CP-even and CP-odd sneutrinos. The mass matrix of a chargino is diagonalized by the rotation matrices U and V.

We also deduce the vertex couplings of a neutrino-slepton-chargino and neutralino-lepton-slepton as

$$\begin{aligned}\mathcal{L}_{\bar{\nu}\chi^-\tilde{L}} =& \bar{\nu}_i\Big((-g_2 U_{j1}^* \sum_{a=1}^{3} U_{ia}^{V*} Z_{ka}^E + U_{j2}^* \sum_{a=1}^{3} U_{ia}^{V*} Y_l^a Z_{k(3+a)}^E) P_L \\ &+ \sum_{a,b=1}^{3} Y_\nu^{ab} U_{i(3+a)}^V Z_{kb}^E V_{j2} P_R\Big)\chi_j^- \tilde{L}_k,\end{aligned} \quad (10)$$

$$\begin{aligned}\mathcal{L}_{\bar{\chi}^0 l\tilde{L}} =& \bar{\chi}_i^0\Big\{\Big(\frac{1}{\sqrt{2}}(g_1 N_{i1}^* + g_2 N_{i2}^* + g_{YX} N_{i5}^*) Z_{kj}^E \\ &- N_{i3}^* Y_l^j Z_{k(3+j)}^E\Big) P_L - \Big[\frac{1}{\sqrt{2}}\big(2 g_1 N_{i1} + (2 g_{YX} + g_X) N_{i5}\big) \\ &\times Z_{k(3+a)}^E + Y_l^j Z_{kj}^E N_{i3}\Big] P_R\Big\} l_j \tilde{L}_k.\end{aligned} \quad (11)$$

Here, Z^E and N are rotation matrices, which can diagonalize the mass squared matrix of the slepton and the mass matrix of the neutralino. The mass matrix of a neutrino is diagonalized using U^V.

Other required couplings can be found in our previous papers [31, 36].

III. FORMULATION

The Feynman amplitude can be expressed by dimension 6 operators [37] using the effective Lagrangian method. Dimension 8 operators can be suppressed by the factor $\frac{m_\mu^2}{M_{\mathrm{SUSY}}^2} \sim (10^{-7}, 10^{-8})$ and then ignored.

These dimension 6 operators are

$$\begin{aligned}O_1^{\mp} &= \frac{1}{(4\pi)^2}\bar{l}(\mathrm{i}\not{\mathcal{D}})^3\omega_{\mp} l, \\ O_2^{\mp} &= \frac{eQ_f}{(4\pi)^2}\overline{(\mathrm{i}\mathcal{D}_\mu l)}\gamma^\mu F\cdot\sigma\omega_{\mp} l, \\ O_3^{\mp} &= \frac{eQ_f}{(4\pi)^2}\bar{l}F\cdot\sigma\gamma^\mu\omega_{\mp}(\mathrm{i}\mathcal{D}_\mu l), \\ O_4^{\mp} &= \frac{eQ_f}{(4\pi)^2}\bar{l}(\partial^\mu F_{\mu\nu})\gamma^\nu\omega_{\mp} l, \\ O_5^{\mp} &= \frac{m_l}{(4\pi)^2}\bar{l}(\mathrm{i}\not{\mathcal{D}})^2\omega_{\mp} l, \\ O_6^{\mp} &= \frac{eQ_f m_l}{(4\pi)^2}\bar{l}F\cdot\sigma\omega_{\mp} l.\end{aligned} \quad (12)$$

Here, $\mathcal{D}_\mu = \partial_\mu + \mathrm{i}eA_\mu$, and $\omega_{\mp} = \frac{1\mp\gamma_5}{2}$. $F_{\mu\nu}$ denotes the electromagnetic field strength, and m_l represents the lepton mass.

The effective Lagrangian of a lepton EDM is

$$\mathcal{L}_{\mathrm{EDM}} = \frac{-\mathrm{i}}{2} d_l \bar{l}\sigma^{\mu\nu}\gamma_5 l F_{\mu\nu}. \quad (13)$$

For Fermions, the EDM cannot be obtained at tree level in the fundamental interaction because it is a CP violation amplitude. Therefore, the one-loop diagrams should have a non-zero contribution to the Fermion EDM in the CP violating electroweak theory. With the relationship between the Wilson coefficients $C_{2,3,6}^{\mp}$ of the operators $O_{2,3,6}^{\mp}$ [26–28, 37], the lepton EDM is obtained as

$$d_l = \frac{-2eQ_f m_l}{(4\pi)^2}\Im(C_2^+ + C_2^{-*} + C_6^+). \quad (14)$$

A. One-loop corrections

The one-loop new physics contributions to lepton EDMs are taken from the diagrams in Fig. 1. The one-loop contributions to lepton EDMs are obtained via calculation with the on-shell condition of the external lepton. Then, we simplify the analytical results.

The analytical results of the one-loop diagrams are shown below.

1. The corrections to lepton EDMs from neutralinos and scalar leptons are

$$d_l^{\tilde{L}\chi^0} = \left(\frac{-e}{2\Lambda}\right)\Im\left[-\sum_{i=1}^{8}\sum_{j=1}^{6}\left\{(A_L^* A_R)\sqrt{x_{\chi_i^0}}x_{\tilde{L}_j}\frac{\partial^2\mathcal{B}(x_{\chi_i^0}, x_{\tilde{L}_j})}{\partial x_{\tilde{L}_j}^2}\right\}\right]. \quad (15)$$

Here, $x_i = \frac{m_i^2}{\Lambda^2}$, where m_i represents the particle mass, and Λ denotes the new physics energy scale. The couplings A_R, A_L can be expressed as

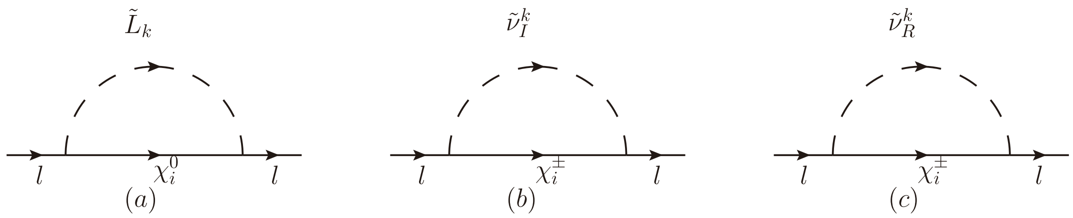

Fig. 1. One-loop self energy diagrams in the $U(1)_X$SSM.

$$A_R = \frac{1}{\sqrt{2}} g_1 N_{i1}^* Z_{j2}^E + \frac{1}{\sqrt{2}} g_2 N_{i2}^* Z_{j2}^E + \frac{1}{\sqrt{2}} g_{YX} N_{i5}^* Z_{j2}^E - N_{i3}^* Y_\mu Z_{j5}^E ,$$
$$A_L = -\frac{1}{\sqrt{2}} Z_{j5}^E (2 g_1 N_{i1} + (2 g_{YX} + g_X) N_{i5}) - Y_\mu^* Z_{j2}^E N_{i3} . \tag{16}$$

The mass matrices of scalar leptons and neutrinos can be diagonalized using the matrices Z^E and N.

The specific forms of the functions $\mathcal{B}(x,y)$ (using Eq. (11)) and $\mathcal{B}_1(x,y)$ (using Eqs. (14) and (16)) are

$$\mathcal{B}(x,y) = \frac{1}{16\pi^2}\left(\frac{x\ln x}{y-x} + \frac{y\ln y}{x-y}\right),$$
$$\mathcal{B}_1(x,y) = \left(\frac{\partial}{\partial y} + \frac{y}{2}\frac{\partial^2}{\partial y^2}\right)\mathcal{B}(x,y) . \tag{17}$$

2. The corrections from the chargino and *CP*-odd scalar neutrino are

$$d_{lI}^{\tilde{\nu}\chi^\pm} = \left(\frac{-e}{2\Lambda}\right)\Im\left[\sum_{i=1}^{2}\sum_{j=1}^{6}\left\{-2(B_L^* B_R)\sqrt{x_{\chi_i^-}}\mathcal{B}_1(x_{\tilde{\nu}_j^I}, x_{\chi_i^-})\right\}\right] . \tag{18}$$

The couplings B_L and B_R can be expressed as

$$B_L = -\frac{1}{\sqrt{2}} U_{i2}^* Z_{j2}^{I*} Y_\mu , \quad B_R = \frac{1}{\sqrt{2}} g_2 Z_{j2}^{I*} V_{i1} . \tag{19}$$

3. The corrections from the chargino and *CP*-even scalar neutrino are

$$d_{lR}^{\tilde{\nu}\chi^\pm} = \left(\frac{-e}{2\Lambda}\right)\Im\left[\sum_{i=1}^{2}\sum_{j=1}^{6}\left\{-2(C_L^* C_R)\sqrt{x_{\chi_i^-}}\mathcal{B}_1(x_{\tilde{\nu}_j^R}, x_{\chi_i^-})\right\}\right] . \tag{20}$$

The couplings C_L and C_R can be expressed as

$$C_L = \frac{1}{\sqrt{2}} U_{i2}^* Z_{j2}^{R*} Y_\mu , \quad C_R = -\frac{1}{\sqrt{2}} g_2 Z_{j2}^{R*} V_{i1} . \tag{21}$$

The U, V, Z^R, and Z^I matrices diagonalize the corresponding particle mass matrices, which are detailed in the appendix.

Therefore, the contributions of the one-loop diagrams to lepton EDMs are

$$d_l^{\text{one-loop}} = d_l^{\tilde{L}\chi^0} + d_{lI}^{\tilde{\nu}\chi^\pm} + d_{lR}^{\tilde{\nu}\chi^\pm} . \tag{22}$$

B. Two-loop corrections

In this paper, the two-loop diagrams that we research include the Barr-Zee two-loop diagrams (Fig. 2 (a), (b), (c)) and rainbow two-loop diagrams (Fig. 2 (d), (e)), as shown below.

The analytical results of the contributions from the two-loop diagrams to lepton EDMs are shown below.

The contributions are taken from Fig. 2 (a). Under the assumption that $m_F = m_{F_1} = m_{F_2} \gg m_W$, the result of simplification [38] is

$$\begin{aligned}
d_l^{WH} = & \frac{-G_F m_W^2 s_W}{256\pi^4} \sum_{F_1=\chi^\pm}\sum_{F_2=\chi^0} \frac{H_{lH\nu}^L}{m_F}\Bigg\{\Im\Bigg[\Bigg[\frac{21}{4} - \frac{5}{18}Q_{F_1} \\
& + \left(3 + \frac{Q_{F_1}}{3}\right)(\ln m_{F_1}^2 - \varrho_{1,1}(m_W^2, m_{H^\pm}^2))\Bigg](H_{HF_1F_2}^L H_{WF_1F_2}^L \\
& + H_{HF_1F_2}^R H_{WF_1F_2}^R) + \Bigg[\frac{19-20Q_{F_1}}{9} + \frac{2-4Q_{F_1}}{3}(\ln m_{F_1}^2 \\
& - \varrho_{1,1}(m_W^2, m_{H^\pm}^2))\Bigg](H_{HF_1F_2}^L H_{WF_1F_2}^R + H_{HF_1F_2}^R H_{WF_1F_2}^L) \\
& + \left[-\frac{16}{9} - \frac{2+6Q_{F_1}}{3}(\ln m_{F_1}^2 - \varrho_{1,1}(m_W^2, m_{H^\pm}^2))\right] \\
& \times (H_{HF_1F_2}^L H_{WF_1F_2}^L - H_{HF_1F_2}^R H_{WF_1F_2}^R) \\
& + \left[-\frac{2Q_{F_1}}{9} - \frac{6-2Q_{F_1}}{3}(\ln m_{F_1}^2 - \varrho_{1,1}(m_W^2, m_{H^\pm}^2))\right] \\
& \times (H_{HF_1F_2}^L H_{WF_1F_2}^R - H_{HF_1F_2}^R H_{WF_1F_2}^L)\Bigg]\Bigg\} .
\end{aligned} \tag{23}$$

Here, $\varrho_{1,1}(x,y) = \dfrac{x\ln x - y\ln y}{x-y}$. $H_{HF_1F_2}^{L,R}$ and $H_{WF_1F_2}^{L,R}$ denote the corresponding couplings coefficients. See Ref. [36] for their concrete forms.

Under the assumption that $m_F = m_{F_1} = m_{F_2} \gg m_{h_0}$, the

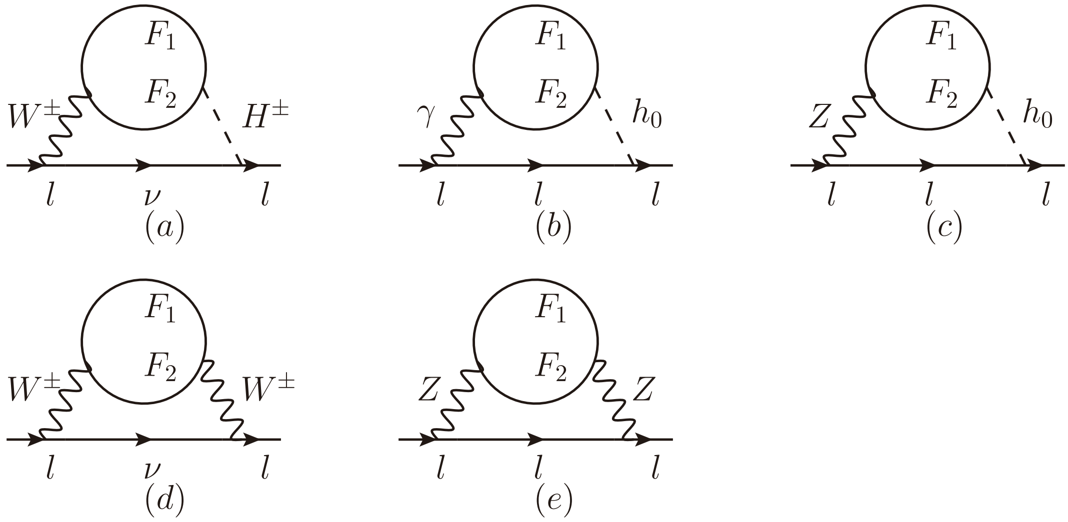

Fig. 2. Two-loop Barr-Zee and rainbow-type diagrams in the $U(1)_X$SSM.

reduced form of the contribution to the lepton EDM from Fig. 2(b) is

$$d_l^{\gamma h_0} = \frac{-eG_F Q_f Q_{F_1} m_W^2 s_W^2}{32\pi^4} \sum_{F_1=F_2=\chi^\pm} \times \left\{ \Im\left[\frac{1}{m_{F_1}} (H^L_{h_0 F_1 F_2}) \left[1 + \ln \frac{m^2_{F_1}}{m^2_{h_0}} \right]\right]\right\}. \tag{24}$$

Moreover, the simplified form from Fig. 2(c) is

$$d_l^{Zh_0} = \frac{-\sqrt{2}e}{1024\pi^4} \sum_{F_1=F_2=\chi^\pm,\chi^0} \left\{ \frac{H_{h_0 l\bar{l}}}{m_{F_1}} \left[\varrho_{1,1}(m_Z^2, m_{h_0}^2) - \ln m^2_{F_1} - 1 \right] \times \Im\left[\left(H^L_{Zll} - H^R_{Zll} \right) \left(H^L_{h_0 F_1 F_2} H^L_{ZF_1F_2} + H^R_{h_0 F_1 F_2} H^R_{ZF_1F_2} \right) \right] \right\}. \tag{25}$$

Here, Q_f represents the electric charge of the external lepton m_μ. Q_{F_1} and Q_{F_2} denote the electric charges of the internal charginos.

With the assumption that $m_F = m_{F_1} = m_{F_2} \gg m_W \sim m_Z$, the reduced form of the contribution to the lepton EDM from Fig. 2(d) is

$$d_l^{WW} = \frac{-eG_F m_l}{384\sqrt{2}\pi^4} \sum_{F_1=\chi^\pm} \sum_{F_2=\chi^0} \left\{ \Im[11(H^{R*}_{WF_1F_2} H^L_{WF_1F_2})] \right\}. \tag{26}$$

We simplify the tedious two-loop results to the order of $\frac{m_\mu^2}{M_Z^2} \sim 10^{-6}$ or $\frac{m_\mu^2}{m^2_{\rm SUSY}}$ under the assumption that $m_F = m_{F1} = m_{F2} \gg m_W \sim m_Z$ and obtain the following simplified form of Fig. 2(e):

$$d_l^{ZZ} = \frac{eQ_{F_1} m_l}{2048\Lambda^2\pi^4} \sum_{F_1=F_2=\chi^\pm} \left\{ \Im\left[(H^L_{ZF_1F_2} H^R_{ZF_1F_2}) \times \left(|H^L_{Zll}|^2 + |H^R_{Zll}|^2 \right) \left[\frac{-6\log x_Z + 6\log x_F + 4}{9x_F} \right] + \left(|H^L_{ZF_1F_2}|^2 + |H^R_{ZF_1F_2}|^2 \right) H^L_{Zll} H^R_{Zll} \times \left[16 \frac{(\log x_F - \log x_Z)(\log x_F + 2) + 2}{x_Z} \right] \right] \right\}. \tag{27}$$

The contributions to lepton EDMs from the researched two-loop diagrams are

$$d_l^{\text{two-loop}} = d_l^{WH} + d_l^{\gamma h_0} + d_l^{Zh_0} + d_l^{WW} + d_l^{ZZ}. \tag{28}$$

At the two-loop level, the contributions to lepton EDMs can be summarized as

$$d_l^{\text{total}} = d_l^{\text{one-loop}} + d_l^{\text{two-loop}}. \tag{29}$$

IV. NUMERICAL RESULTS

For the numerical discussion, we consider the following experimental limitations. The lightest *CP*-even higgs mass is considered as an input parameter, which is $m_{h^0} \approx 125.1$ GeV [39, 40], and the h^0 decays are $h^0 \to \gamma+\gamma$, $h^0 \to Z+Z$, and $h^0 \to \gamma+\gamma$ [41]. Experimental constraints on the masses of the new particles are also considered. LHC experiments have more stringent mass constraints on the Z' boson. To satisfy this experimental constraint, we take the parameter $M_{Z'}$ to be greater than 5.1 TeV [42], which is heavier than the previous mass limit. The ratio of $M_{Z'}$ to its gauge coupling g_X ($\frac{M_{Z'}}{g_X}$) should not be less than 6 TeV at the 99% C.L. [43, 44]. Considering the constraints from the LHC, we set $\tan\beta_\eta < 1.5$ [45]. Because $M_{Z'}$ has a large mass, the contribution of Z' at the amplitude level is small; therefore, the contribution of Z' is ignored. We adjust the parameters based on the experimental limitation of lepton EDMs. In this section, we research and discuss lepton (e,μ,τ) EDMs.

The parameters used in the $U(1)_X$SSM are

$$\begin{aligned}
&g_X = 0.33,\ \ g_{YX} = 0.2,\ \ \lambda_C = -0.1,\ \ \kappa = 0.1,\\
&T_{\lambda_H} = 1.0\ \mathrm{TeV},\ \ T_\kappa = 1.0\ \mathrm{TeV},\ \ \tan\beta_\eta = 1.05,\\
&v_\eta = 15\times\cos\beta_\eta\ \mathrm{TeV},\ \ v_{\bar\eta} = 15\times\sin\beta_\eta\ \mathrm{TeV},\ B_\mu = 8\ \mathrm{TeV}^2,\\
&m_S^2 = 8\ \mathrm{TeV}^2, T_{\lambda_C} = 150\ \mathrm{GeV}, T_{E11} = T_{E22} = T_{E33} = 0.1\ \mathrm{TeV},\\
&M_{\nu11} = M_{\nu22} = M_{\nu33} = 6\ \mathrm{TeV}^2,\ Y_{X11} = Y_{X22} = Y_{X33} = 0.04,\\
&B_S = 8\ \mathrm{TeV}^2,\ \lambda_H = 0.1,\ l_W = 8\ \mathrm{TeV}^2,\\
&T_{X11} = T_{X22} = T_{X33} = 10\ \mathrm{GeV}.
\end{aligned} \tag{30}$$

θ_1, θ_2, and θ_μ are the *CP* violating phases of the parameters m_1, m_2, and μ. We consider three new *CP* violating parameters with the phases θ_{BL}, $\theta_{BB'}$, and θ_S.

$$\begin{aligned}
&m_1 = M_1 * \mathrm{e}^{\mathrm{i}*\theta_1},\ \ m_2 = M_2 * \mathrm{e}^{\mathrm{i}*\theta_2},\ \ \mu = mu * \mathrm{e}^{\mathrm{i}*\theta_\mu},\\
&m_{BL} = M_{BL} * \mathrm{e}^{\mathrm{i}*\theta_{BL}},\ \ m_{BB'} = M_{BB'} * \mathrm{e}^{\mathrm{i}*\theta_{BB'}},\\
&m_S = M_S * \mathrm{e}^{\mathrm{i}*\theta_S}.
\end{aligned} \tag{31}$$

To facilitate the discussion, we make the following simplifications:

$$\begin{aligned}
&M_L = M_{L11} = M_{L22} = M_{L33},\\
&M_E = M_{E11} = M_{E22} = M_{E33},\\
&T_E = T_{E11} = T_{E22} = T_{E33}.
\end{aligned} \tag{32}$$

A. *e* EDM

Previously, we discussed the EDM of electrons because of its strict experimental upper limit. The CP violating phases θ_1, θ_2, θ_μ, θ_{BL}, $\theta_{BB'}$, and θ_S as well as other parameters have a certain impact on the electron EDM. Now, supposing $\theta_1 = \theta_2 = \theta_\mu = \theta_{BB'} = \theta_S = 0$, and setting $\tan\beta = 5$, $M_2 =$ 500 GeV, $mu =$ 500 GeV, $M_{BL} =$ 1800 GeV, $M_{BB'} =$ 700 GeV, $M_S =$ 2400 GeV, $M_L =$ 1.1 TeV, $M_E =$ 1.0 TeV. We study the influence of θ_{BL}on the electron EDM. M_{BL} is related to the neutralino mass matrix. In Fig. 3, we plot a solid line and dashed line versus M_L $(0.9\sim1.1\ \mathrm{TeV}^2)$ corresponding to M_1 = 700 and 800 GeV. We can see that these two lines are subtractive functions and θ_{BL} has an influence on $|d_e|$. The relationship between d_e and M_L is not a simple linear relation; its change curve follows M_L^{-2}. The shaded part of the figure

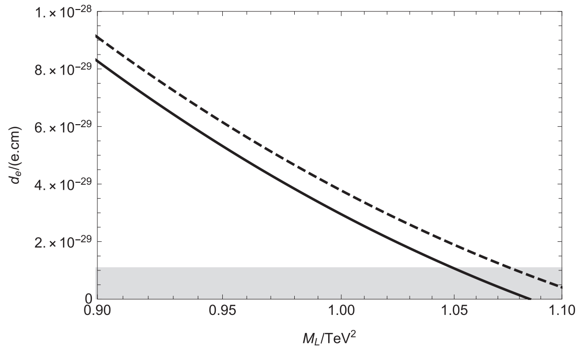

Fig. 3. Setting $\theta_1 = \theta_2 = \theta_\mu = \theta_{BB'} = \theta_S = 0$ and $\theta_{BL} = \frac{\pi}{4}$, the contributions to the electron EDM varying with M_L are plotted. The solid and dashed lines correspond to M_1 = (700, 800) GeV, respectively.

indicates that all these parameters are reasonable and conform to experimental limits.

Setting $\theta_1 = \theta_2 = \theta_\mu = \theta_{BB'} = \theta_{BL} = 0$, $\tan\beta = 5$, $M_1 =$ 700 GeV, $M_2 =$ 2000 GeV, $mu =$ 500 GeV, $M_{BL} =$ 1600 GeV, $M_{BB'} =$ 800 GeV, $M_S = -800$ GeV, $M_{L22} = 1.0$ TeV², and $M_E = 1.0$ TeV², we consider the impact of θ_S on the electron EDM. M_S is related to the mass matrices of the neutralino and scalar lepton. In Fig. 4, M_{L11} varies from 0.5 to 5.0 TeV², and when $M_{L11} > 2.0$ TeV², the numerical results of $|d_e|$ conform to the experimental limits.

$\theta_{BB'}$ is the new *CP* violating phase of the lepton neutrino mass matrix. Therefore, it offers a new physical contribution to the lepton EDM. Setting $\theta_1 = \theta_2 = \theta_\mu = \theta_S = \theta_{BL} = 0$, the contributions to the muon EDM varying with T_E are plotted, with the solid and dashed lines corresponding to $M_{E11} = 0.5$ and 1.0 TeV², respectively. Here, we set $\tan\beta = 5$, $M_1 = 700$ GeV, $M_2 = 2000$ GeV, $mu = 500$ GeV, $M_{BL} =$ 1800 GeV, $M_{BB'} =$ 700 GeV, $M_S =$ 2400 GeV, $M_L =$ 1.0 TeV², and $M_E = 0.5$ TeV². In Fig. 5, the two lines are shaped like parabolas, and most of the numerical results are within the experimental limits.

We select the parameters $M_{L11}(0.5\sim5.0\ \mathrm{TeV}^2)$, $M_{L22}(0.5\sim5.0\ \mathrm{TeV}^2)$, $M_{L33}(0.5\sim5.0\ \mathrm{TeV}^2)$, $T_E(-3000\sim$

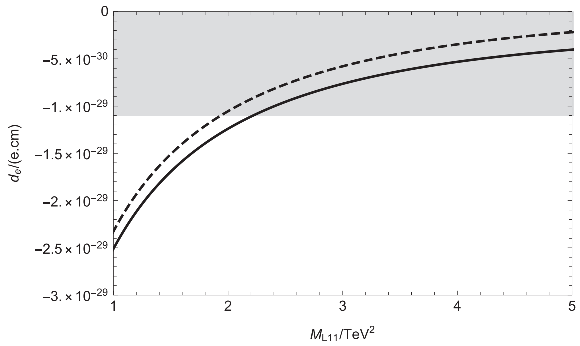

Fig. 4. Setting $\theta_1 = \theta_2 = \theta_\mu = \theta_{BB'} = \theta_{BL} = 0$ and $\theta_S = \frac{\pi}{4}$, the contributions to the electron EDM varying with M_{L11} are plotted. The solid and dashed lines correspond to M_{L33} = (1, 0.9) TeV², respectively.

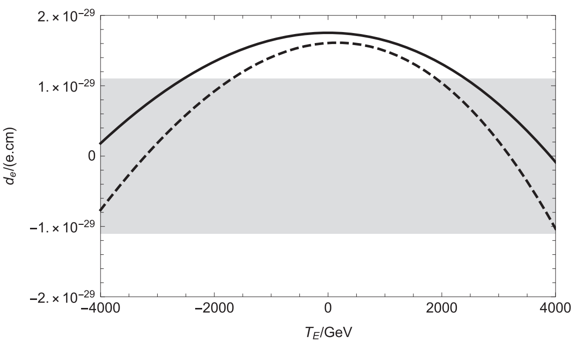

Fig. 5. Setting $\theta_1 = \theta_2 = \theta_\mu = \theta_S = \theta_{BL} = 0$ and $\theta_{BB'} = \frac{\pi}{3}$, the contributions to the electron EDM varying with T_E are plotted. The solid and dashed lines correspond to $M_{E11} = (0.5, 1.0)$ TeV^2, respectively.

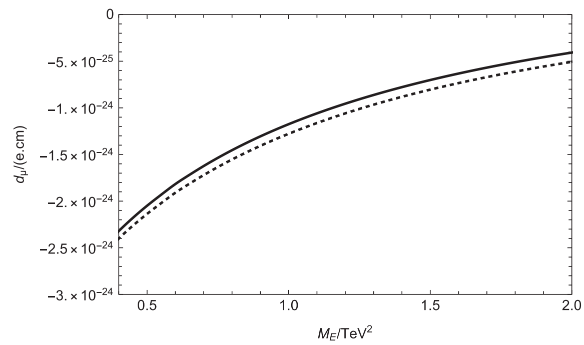

Fig. 7. Setting $\theta_1 = \theta_2 = \theta_\mu = \theta_{BB'} = \theta_{BL} = 0$ and $\theta_S = \frac{\pi}{3}$, the contributions to the muon EDM varying with M_E are plotted. The solid and dashed lines correspond to $M_{BL} = (1200, 1500)$ GeV.

3000 GeV), and $M_E(0.5 \sim 5.0$ TeV^2) and randomly scatter the points. With $\theta_1 = \theta_2 = \theta_\mu = \theta_{BB'} = \theta_{BL} = 0$ and $\theta_S = \frac{\pi}{4}$, we plot $|d_e|$ in the plane of M_{L11} versus M_{L22} in Fig. 6. "■" represents $|d_e| < 1.1\times10^{-29}$ e.cm, and "∘" represents $|d_e| \geqslant 1.1\times10^{-29}$ e.cm. In Fig. 6, we can see that there is clear stratification. When $M_{L11} > 1.0$ TeV^2, M_{L22} is in the vicinity of 1.4 TeV^2, $|d_e|$ is within the experimental limit. This reveals that M_{L11} is a sensitive parameter and M_{L22} is a less sensitive parameter.

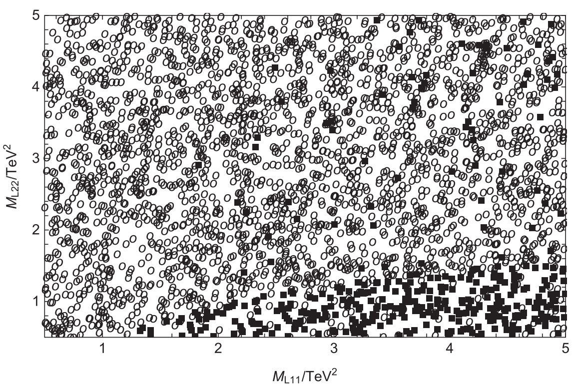

Fig. 6. With $\theta_1 = \theta_2 = \theta_\mu = \theta_{BB'} = \theta_{BL} = 0$ and $\theta_S = \frac{\pi}{4}$, $|d_e|$ is in the plane of M_{L11} versus M_{L22}. "■" represents $|d_e| < 1.1\times10^{-29}$ e.cm, "∘" represents $|d_e| \geqslant 1.1\times10^{-29}$ e.cm.

B. μ EDM

In this section, the muon EDM is numerically studied. In Fig. 7, setting $\theta_1 = \theta_\mu = \theta_{BB'} = \theta_2 = \theta_{BL} = 0$ and $\tan\beta = 6$, $M_1 = 1450$ GeV, $M_2 = 2000$ GeV, $mu = 500$ GeV, $M_{BB'} = 800$ GeV, $M_S = -800$ GeV, $M_L = 1.0$ TeV^2, and $M_E = 0.5$ TeV^2. We study the influence of θ_S on the muon EDM. The solid and dashed lines correspond to M_{BL} (1200, 1500 GeV), respectively. From the numerical results, we can see that the muon EDM increases as M_E increases. θ_S has a significant influence on the numerical results because M_S is related to the mass matrices of the neutralino and charged Higgs.

$\theta_{BB'}$ is the new *CP* violating phase of the neutralino mass matrix. Therefore, it offers a new physical contribution to the lepton EDMs. With $\theta_1 = \theta_2 = \theta_\mu = \theta_S = \theta_{BL} = 0$, the contributions to the muon EDM varying with M_{E22} are plotted, where the solid and dashed lines correspond to $\tan\beta = (5, 6)$, respectively. In this part, we set $M_1 = 1450$ GeV, $M_2 = 800$ GeV, $mu = 500$ GeV, $M_{BL} = 1600$ GeV, $M_{BB'} = 800$ GeV, $M_S = -800$ GeV, $M_L = 1.0$ TeV^2, and $M_E = 0.5$ TeV^2. In Fig. 8, as M_{E22} increases, the numerical results gradually decrease, and the shapes of the two lines are similar.

We choose the parameters $M_{L11}(0.5 \sim 5.0$ TeV^2), $M_{L22}(0.5 \sim 5.0$ TeV^2), $M_{L33}(0.5 \sim 5.0$ TeV^2), $T_E(-3000 \sim 3000$ GeV), and $M_E(0.5 \sim 5.0$ TeV^2) and randomly scatter the points. With $\theta_1 = \theta_2 = \theta_\mu = \theta_{BB'} = \theta_{BL} = 0$, and $\theta_S = \frac{\pi}{4}$, we study $|d_\mu|$ in the plane of M_{L33} versus M_E. In Fig. 9, "■" represents $|d_\mu| < 1\times10^{-24}$ e.cm, and "∘" represents $|d_\mu| \geqslant 1\times10^{-24}$ e.cm. Delamination occurs when $M_E = 1.1$ TeV^2, and stratification is clear. This reveals that M_E is a sensitive parameter and M_{L33} is an insensitive parameter. These parameters are in a reasonable parameter space.

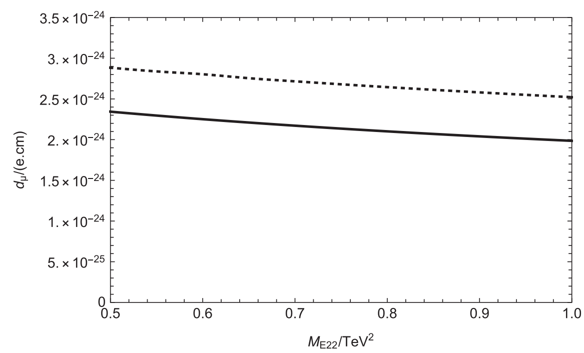

Fig. 8. Setting $\theta_1 = \theta_2 = \theta_\mu = \theta_S = \theta_{BL} = 0$ and $\theta_{BB'} = \frac{\pi}{6}$, the contributions to the muon EDM varying with M_{E22} are plotted. The solid and dashed lines correspond to $\tan\beta = (5, 6)$.

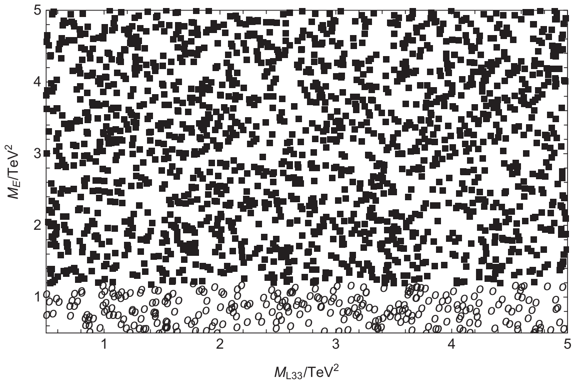

Fig. 9. With $\theta_1 = \theta_2 = \theta_\mu = \theta_{BB'} = \theta_{BL} = 0$ and $\theta_S = \frac{\pi}{4}$, $|d_\mu|$ is in the plane of M_{L33} versus M_E, where "■" represents $|d_\mu| < 1\times10^{-24}$ e.cm, and "∘" represents $|d_\mu| \geqslant 1\times10^{-24}$ e.cm.

C. τ EDM

At present, the experimental upper bound of the tau EDM is $|d_\tau^{\exp}| < 1.1\times10^{-17}$ e.cm, which is largest among the bounds of lepton EDMs. Therefore, we now study the tau EDM. With $\tan\beta = 6$, $M_1 = 750$ GeV, $mu = 650$ GeV, $M_{BL} = 1800$ GeV, $M_{BB'} = 700$ GeV, $M_S = 1400$ GeV, $M_L = 1.0\,\text{TeV}^2$, and $M_E = 1.0\,\text{TeV}^2$ and setting $\theta_1 = \theta_2 = \theta_\mu = \theta_{BB'} = \theta_{BL} = 0$ and $\theta_S = \frac{\pi}{5}$, we study the influence of M_{L33} on $|d_\tau|$. In Fig. 10, the solid and dashed lines correspond to $M_2 = (400, 500$ GeV), respectively, and their numerical results are all in the negative. The two lines are increasing functions of M_{L33}, and θ_S has clearer influence on the numerical result of $|d_\tau|$. The maximum value of the two lines reaches 5.0×10^{-23} e.cm, and this value is six orders of magnitude smaller than the upper limit of the experiment.

θ_{BL} is the new *CP* violating phase of M_{BL} in the neutralino mass matrix. Setting $\tan\beta = 6$, $M_1 = 750$ GeV, $M_2 = 400$ GeV, $M_{BL} = 1800$ GeV, $M_{BB'} = 700$ GeV, $M_S = 1400$ GeV, $M_E = 1.0\,\text{TeV}^2$, $\theta_1 = \theta_2 = \theta_\mu = \theta_{BB'} = \theta_S = 0$, and $\theta_{BL} = \frac{\pi}{6}$, the contributions to the tau EDM varying with M_L are plotted, where the solid and dashed lines correspond to $mu = (650, 750\,\text{GeV})$, respectively. In Fig. 11, we can see that $|d_\tau|$ decreases with increasing M_L. The maximum value of these two lines reaches $|d_\tau| = 4.5\times10^{-23}$ e.cm.

We select the parameters $M_{L11}(0.5\sim5.0\,\text{TeV}^2)$, $M_{L22}(0.5\sim5.0\,\text{TeV}^2)$, $M_{L33}(0.5\sim5.0\,\text{TeV}^2)$, $T_E(-3000\sim3000\,\text{GeV})$, and $\tan\beta(2\sim20)$ and randomly scatter the points. In Fig. 12, we study $|d_\tau|$ in the plane of M_{L33} and $\tan\beta$ to observe their influence. The varying regions of M_{L33} and $\tan\beta$ are in the range $(0.5\sim5\,\text{TeV}^2)$ and $(2\sim20)$, respectively."■" represents $|d_\tau| < 1\times10^{-23}$ e.cm, and "∘" represents $|d_\tau| \geqslant 1\times10^{-23}$ e.cm. When $\tan\beta = 6$, stratification occurs, and the stratification is more clear. This indicates that $\tan\beta$ is a sensitive parameter.

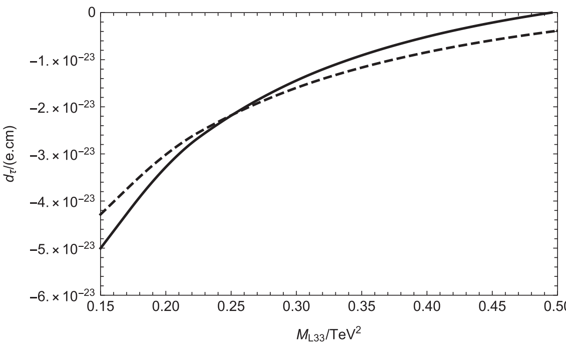

Fig. 10. Setting $\theta_1 = \theta_2 = \theta_\mu = \theta_{BB'} = \theta_{BL} = 0$ and $\theta_S = \frac{\pi}{5}$, the contributions to the tau EDM varying with M_{L33} are plotted. The solid and dashed lines correspond to $M_2 = (400, 500)$ GeV, respectively.

V. DISCUSSION AND CONCLUSION

In the $U(1)_X$SSM, we calculate and analyze one-loop and two-loop contributions to lepton (e, μ, τ) EDMs. The effects of the *CP* violating phases θ_1, θ_2, θ_μ, $\theta_{BB'}$, θ_S, and θ_{BL} on the lepton EDMs are researched. Among them, $\theta_{BB'}$, θ_S, and θ_{BL} are all newly introduced. The experimental upper limit of the electron EDM is

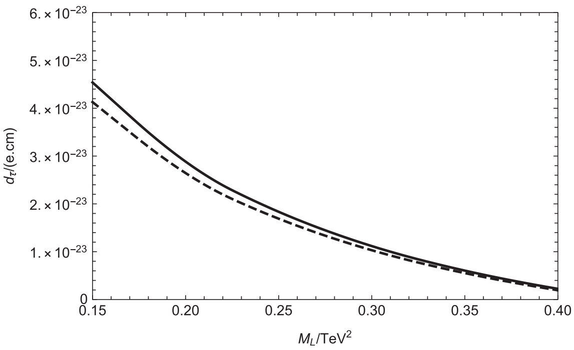

Fig. 11. Setting $\theta_1 = \theta_2 = \theta_\mu = \theta_S = \theta_{BB'} = 0$ and $\theta_{BL} = \frac{\pi}{6}$, the contributions to the tau EDM varying with M_L are plotted. The solid and dashed lines correspond to $mu = (650, 750)$ GeV.

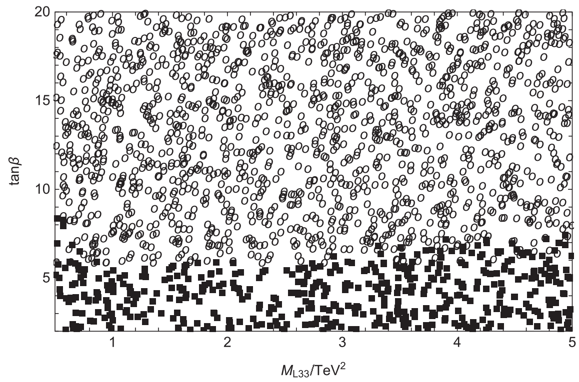

Fig. 12. With $\theta_1 = \theta_2 = \theta_\mu = \theta_{BB'} = \theta_S = 0$ and $\theta_{BL} = \frac{\pi}{6}$, $|d_\tau|$ is in the plane of M_{L33} versus $\tan\beta$. "■" represents $|d_\tau| < 1\times10^{-23}$ e.cm, and "∘" represents $|d_\tau| \geqslant 1\times10^{-23}$ e.cm.

$|d_e^{\rm exp}| < 1.1\times10^{-29}$ e.cm, which places strict restrictions on the $U(1)_X$SSM parameter space. In the parameter space used in this study, the numerical result for $|d_e|$ can be controlled below the experimental limit. In our study, the largest numerical results for the μ EDM and τ EDM are approximately 2.8×10^{-24} e.cm and 5.0×10^{-23} e.cm, respectively. They are all in a reasonable parameter space and do not exceed the upper limit of the experiment. For the corrections of the lepton EDMs, the one-loop contributions are dominant. As for the one-loop and two-loop contributions to the EDMs, their relative size $(d_l^{\rm two-loop}/d_l^{\rm one-loop})$ is approximately 5% ~ 15% after numerical calculation.

Our numerical results mainly obey the rule $d_e/d_\mu/d_\tau \sim m_e/m_\mu/m_\tau$. In Fig. 3, when $\theta_{BL} = \frac{\pi}{4}$, M_L has a more obvious impact on the electron EDM, and the influence of θ_{BL} on the electron EDM is also more obvious. In addition, the influences of the CP-violating phases θ_S and $\theta_{BB'}$ on lepton EDMs are clear. In Fig. 7, when $\theta_S = \frac{\pi}{3}$, the value of the muon EDM increases as M_E increases (the numerical results are all negative). θ_S has a significant influence on the numerical results because M_S is related to the mass matrices of the neutralino and charged Higgs. In Fig. 8, when $\theta_{BB'} = \frac{\pi}{6}$, the two lines (solid and dashed lines) are decreasing functions of M_{E22}. The above parameters (M_L, M_E) are all elements on the diagonal of the mass matrix; therefore, their corresponding results are all decoupled, such as in Fig. 3, Fig. 4, Fig. 7, Fig. 8, Fig. 10, and Fig. 11. In Fig. 12, We can see that $|d_\tau|$ increases with increasing $\tan\beta$. If we use the method of mass insertion [46] to analyze the results, we can intuitively find that $\tan\beta$ is proportional to lepton EDMs. We also perform random spot operations on lepton EDMs. The randomly scattered pictures exhibit clear stratification, which also helps us find a reasonable parameter space. As the accuracy of technology improves in the near future, lepton EDMs may be detected.

APPENDIX A

The mass matrix for a slepton with the basis $(\tilde{e}_L, \tilde{e}_R)$

$$m_{\tilde{e}}^2 = \begin{pmatrix} m_{\tilde{e}_L\tilde{e}_L^*} & \frac{1}{2}(\sqrt{2}v_d T_e^\dagger - v_u(\lambda_H v_S + \sqrt{2}\mu)Y_e^\dagger) \\ \frac{1}{2}(\sqrt{2}v_d T_e - v_u Y_e(\sqrt{2}\mu^* + v_S\lambda_H^*)) & m_{\tilde{e}_R\tilde{e}_R^*} \end{pmatrix}, \tag{A1}$$

$$\begin{aligned} m_{\tilde{e}_L\tilde{e}_L^*} &= m_{\tilde{l}}^2 + \frac{1}{8}\Big((g_1^2 + g_{YX}^2 + g_{YX}g_X - g_2^2)(v_d^2 - v_u^2) + 2g_{YX}g_X(v_\eta^2 - v_{\bar{\eta}}^2)\Big) + \frac{1}{2}v_d^2 Y_e^\dagger Y_e, \\ m_{\tilde{e}_R\tilde{e}_R^*} &= m_{\tilde{e}}^2 - \frac{1}{8}\Big([2(g_1^2 + g_{YX}) + 3g_{YX}g_X + g_X^2](v_d^2 - v_u^2) + (4g_{YX}g_X + 2g_X^2)(v_\eta^2 - v_{\bar{\eta}}^2)\Big) + \frac{1}{2}v_d^2 Y_e Y_e^\dagger . \end{aligned} \tag{A2}$$

This matrix is diagonalized by Z^E

$$Z^E m_{\tilde{e}}^2 Z^{E,\dagger} = m_{2,\tilde{e}}^{\rm dia} . \tag{A3}$$

The mass matrix for a CP-even sneutrino (ϕ_l, ϕ_r) reads as

$$m_{\tilde{\nu}^R}^2 = \begin{pmatrix} m_{\phi_l\phi_l} & m_{\phi_r\phi_l}^T \\ m_{\phi_l\phi_r} & m_{\phi_r\phi_r} \end{pmatrix}, \tag{A4}$$

$$m_{\phi_l\phi_l} = \frac{1}{8}\Big((g_1^2 + g_{YX}^2 + g_2^2 + g_{YX}g_X)(v_d^2 - v_u^2) + g_{YX}g_X(2v_\eta^2 - 2v_{\bar{\eta}}^2)\Big) + \frac{1}{2}v_u^2 Y_\nu^T Y_\nu + m_{\tilde{L}}^2 , \tag{A5}$$

$$m_{\phi_l\phi_r} = \frac{1}{\sqrt{2}}v_u T_\nu + v_u v_{\bar{\eta}} Y_X Y_\nu - \frac{1}{2}v_d(\lambda_H v_S + \sqrt{2}\mu)Y_\nu , \tag{A6}$$

$$m_{\phi_r\phi_r} = \frac{1}{8}\Big((g_{YX}g_X + g_X^2)(v_d^2 - v_u^2) + 2g_X^2(v_\eta^2 - v_{\bar{\eta}}^2)\Big) + v_\eta v_S Y_X \lambda_C + m_{\tilde{\nu}}^2 + \frac{1}{2}v_u^2|Y_\nu|^2 + v_{\bar{\eta}}(2v_{\bar{\eta}}|Y_X|^2 + \sqrt{2}T_X) . \tag{A7}$$

This matrix is diagonalized by Z^R

$$Z^R m^2_{\tilde{\nu}^R} Z^{R,\dagger} = m^{\rm dia}_{2,\tilde{\nu}^R} \,. \tag{A8}$$

The mass matrix for a CP-odd sneutrino (σ_l, σ_r) is deduced as

$$m^2_{\tilde{\nu}^I} = \begin{pmatrix} m_{\sigma_l\sigma_l} & m^T_{\sigma_r\sigma_l} \\ m_{\sigma_l\sigma_r} & m_{\sigma_r\sigma_r} \end{pmatrix}, \tag{A9}$$

$$m_{\sigma_l\sigma_l} = \frac{1}{8}\Big((g_1^2+g_{YX}^2+g_2^2+g_{YX}g_X)(v_d^2-v_u^2)+2g_{YX}g_X(v_\eta^2-v_{\bar\eta}^2)\Big)+\frac{1}{2}v_u^2 Y_\nu^T Y_\nu + m_{\tilde L}^2 \,, \tag{A10}$$

$$m_{\sigma_l\sigma_r} = \frac{1}{\sqrt{2}}v_u T_\nu - v_u v_{\bar\eta} Y_X Y_\nu - \frac{1}{2}v_d(\lambda_H v_S + \sqrt{2}\mu)Y_\nu, \tag{A11}$$

$$m_{\sigma_r\sigma_r} = \frac{1}{8}\Big((g_{YX}g_X+g_X^2)(v_d^2-v_u^2)+2g_X^2(v_\eta^2-v_{\bar\eta}^2)\Big)-v_\eta v_S Y_X\lambda_C + m_{\tilde\nu}^2+\frac{1}{2}v_u^2|Y_\nu|^2+v_{\bar\eta}(2v_{\bar\eta}Y_X Y_X-\sqrt{2}T_X) \,. \tag{A12}$$

This matrix is diagonalized by Z^I

$$Z^I m^2_{\tilde{\nu}^I} Z^{I,\dagger} = m^{dia}_{2,\tilde{\nu}^I} \,. \tag{A13}$$

The mass matrix for charginos in the basis $(\tilde{W}^-, \tilde{H}_d^-), (\tilde{W}^+, \tilde{H}_u^+)$

$$m_{\tilde{\chi}^-} = \begin{pmatrix} M_2 & \frac{1}{\sqrt{2}}g_2 v_u \\ \frac{1}{\sqrt{2}}g_2 v_d & \frac{1}{\sqrt{2}}\lambda_H v_S + \mu \end{pmatrix}, \tag{A14}$$

The matrix is diagonalized by U and V

$$U^* m_{\tilde{\chi}^-} V^\dagger = m^{\rm dia}_{\tilde{\chi}^-}. \tag{A15}$$

The mass matrix for charged Higgs in the basis $(H_d^-, H_u^{+,*}), (H_d^{-,*}, H_u^+)$

$$m^2_{H^-} = \begin{pmatrix} m_{H_d^- H_d^{-,*}} & m^*_{H_u^{+,*} H_d^{-,*}} \\ m_{H_d^- H_u^+} & m_{H_u^{+,*} H_u^+} \end{pmatrix}, \tag{A16}$$

$$\begin{aligned} m_{H_d^- H_d^{-,*}} =& \frac{1}{8}((g_2^2+g_X^2)v_d^2+(-g_X^2+g_2^2)v_u^2+(g_1^2+g_{YX}^2)(-v_u^2+v_d^2)-2g_X^2v_{\bar\eta}^2+2(g_{YX}g_X(-v_{\bar\eta}^2-v_u^2+v_d^2+v_\eta^2)+g_X^2v_\eta^2) \\ &+\frac{1}{2}(2\,|\,\mu\,|^2+2\sqrt{2}v_S\,\Re(\mu\lambda_H^*)+v_S^2\,|\,\lambda_H\,|^2 \,, \end{aligned} \tag{A17}$$

$$m_{H_d^- H_u^+} = \frac{1}{2}(2(\lambda_H l_W^* + B_\mu)+\lambda_H(2\sqrt{2}v_S M_S^* - v_d v_u \lambda_H^* + v_\eta v_{\bar\eta}\lambda_C^* + \sqrt{2}v_S T_{\lambda_H})) + \frac{1}{4}g_2^2 v_d v_u \,, \tag{A18}$$

$$\begin{aligned} m_{H_u^{+,*} H_u^+} =& \frac{1}{8}((-g_X^2+g_2^2)v_d^2+(g_2^2+g_X^2)v_u^2+(g_1^2+g_{YX}^2)(-v_d^2+v_u^2)-2g_X^2v_\eta^2+2(g_{YX}g_X(-v_d^2-v_\eta^2+v_u^2+v_{\bar\eta}^2)+g_X^2v_{\bar\eta}^2)) \\ &+\frac{1}{2}(2\,|\,\mu\,|^2+2\sqrt{2}v_S\,\Re(\mu\lambda_H^*)+v_S^2\,|\,\lambda_H\,|^2) \,. \end{aligned} \tag{A19}$$

This matrix is diagonalized by Z^+

$$Z^+ m^2_{H^-} Z^{+,\dagger} = m^{\text{dia}}_{2,H^-} \ . \tag{A20}$$

The mass matrix for a neutralino in the basis $(\lambda_{\tilde{B}}, \tilde{W}^0, \tilde{H}_d^0, \tilde{H}_u^0, \lambda_{\tilde{X}}, \tilde{\eta}, \tilde{\bar{\eta}}, \tilde{s})$ is

$$m_{\tilde{\chi}^0} = \begin{pmatrix} M_1 & 0 & -\frac{g_1}{2}v_d & \frac{g_1}{2}v_u & M_{BB'} & 0 & 0 & 0 \\ 0 & M_2 & \frac{g_2}{2}v_d & -\frac{g_2}{2}v_u & 0 & 0 & 0 & 0 \\ -\frac{g_1}{2}v_d & \frac{g_2}{2}v_d & 0 & m_{\tilde{H}_u^0\tilde{H}_d^0} & m_{\lambda_{\tilde{X}}\tilde{H}_d^0} & 0 & 0 & -\frac{\lambda_H v_u}{\sqrt{2}} \\ \frac{g_1}{2}v_u & -\frac{g_2}{2}v_u & m_{\tilde{H}_d^0\tilde{H}_u^0} & 0 & m_{\lambda_{\tilde{X}}\tilde{H}_u^0} & 0 & 0 & -\frac{\lambda_H v_d}{\sqrt{2}} \\ M_{BB'} & 0 & m_{\tilde{H}_d^0\lambda_{\tilde{X}}} & m_{\tilde{H}_u^0\lambda_{\tilde{X}}} & M_{BL} & -g_X v_\eta & g_X v_{\bar{\eta}} & 0 \\ 0 & 0 & 0 & 0 & -g_X v_\eta & 0 & \frac{1}{\sqrt{2}}\lambda_C v_S & \frac{1}{\sqrt{2}}\lambda_C v_{\bar{\eta}} \\ 0 & 0 & 0 & 0 & g_X v_{\bar{\eta}} & \frac{1}{\sqrt{2}}\lambda_C v_S & 0 & \frac{1}{\sqrt{2}}\lambda_C v_\eta \\ 0 & 0 & -\frac{1}{\sqrt{2}}\lambda_H v_u & -\frac{1}{\sqrt{2}}\lambda_H v_d & 0 & \frac{1}{\sqrt{2}}\lambda_C v_{\bar{\eta}} & \frac{1}{\sqrt{2}}\lambda_C v_\eta & m_{\tilde{s}\tilde{s}} \end{pmatrix}, \tag{A21}$$

$$\begin{aligned} & m_{\tilde{H}_d^0\tilde{H}_u^0} = -\frac{1}{\sqrt{2}}\lambda_H v_S - \mu, \ \ m_{\tilde{H}_d^0\lambda_{\tilde{X}}} = -\frac{1}{2}(g_{YX}+g_X)v_d, \\ & m_{\tilde{H}_u^0\lambda_{\tilde{X}}} = \frac{1}{2}(g_{YX}+g_X)v_u, \ \ m_{\tilde{s}\tilde{s}} = 2M_S + \sqrt{2}\kappa v_S \ . \end{aligned} \tag{A22}$$

This matrix is diagonalized by N,

$$N^* m_{\tilde{\chi}^0} N^\dagger = m^{\text{dia}}_{\tilde{\chi}^0} \ . \tag{A23}$$

References

[1] N.F. Ramsey, Rept. Prog. Phys. **45**, 95-113 (1982)
[2] A. Shindler, Eur. Phys. J. A **57**, 128 (2021)
[3] J. Baron *et al.*, (ACME Collaboration), Science **343**, 269 (2014)
[4] V. Andreev *et al.*, (ACME Collaboration), Nature **562**, 355-60 (2018)
[5] A. Crivellin, M. Hoferichter, and P.S. Wellenburg, Phys. Rev. D **98**, 113002 (2018)
[6] P.A. Zyla *et al.*, (Particle Data Group), PTEP **8**, 083-01 (2020)
[7] F. del Aguila, M. B. Gavela, J. A. Grifols *et al.*, Phys. Lett. B **126**, 71-73 (1983) [Erratum: Phys. Lett. B **129**, 473 (1983)]
[8] T. Ibrahim and P. Nath, Phys. Rev. D **58**, 111301 (1998)
[9] S. Atag and E. Gurkanli, JHEP **1606**, 118 (2016)
[10] T. Abe, N. Omoto, O. Seto *et al.*, Phys. Rev. D **98**, 075029 (2018)
[11] J. Rosiek, Phys.Rev. D **41**, 3464 (1990)
[12] H.P. Nilles, Phys. Rept. **110**, 1 (1984)
[13] H.E. Haber and G.L. Kane, Phys. Rept. **117**, 75 (1985)
[14] S.M. Zhao, T.F. Feng, X.J. Zhan *et al.*, JHEP **07**, 124 (2015)
[15] F. Staub, SARAH, (2008) arXiv: 0806.0538
[16] F. Staub, Comput. Phys. Commun. **185**, 1773 (2014)
[17] F. Staub, Adv. High Energy Phys. **2015**, 840780 (2015)
[18] M. Carena, J.R. Espinosaos, C.E.M. Wagner *et al.*, Phys. Lett. B **355**, 209 (1995)
[19] M. Carena, S. Gori, N.R. Shah *et al.*, JHEP **1203**, 014 (2012)
[20] S. Heinemeyer, D. Stockinger, and G. Weiglein, Nucl. Phys. B **699**, 103 (2004)
[21] T.F. Feng, T. Huang, X.Q. Li *et al.*, Phys. Rev. D **68**, 016004 (2003)
[22] M. Pospelov and A. Ritz, Annals Phys. **318**, 119-169 (2005)
[23] T. Abe, J. Hisano, T. Kitahara *et al.*, JHEP **1401**, 106 (2014)

[24] S. Ipek, Phys. Rev. D **89**, 073012 (2014)
[25] W. Bernreuther, L. Chen, and O. Nachtmann, Phys. Rev. D **103**, 096011 (2021)
[26] A. Pilaftsis, Phys. Rev. D **58**, 096010 (1998)
[27] M. Carena, J. Ellis, A. Pilaftsis *et al.*, Nucl. Phys. B **586**, 92 (2000)
[28] N. Yamanaka, Phys. Rev. D **87**, 011701 (2013)
[29] X.G. He, C.J. Lee, S.F. Li *et al.*, JHEP **1408**, 019 (2014)
[30] X.G. He, C.J. Lee, S.F. Li *et al.*, Phys. Rev. D **89**, 091901 (2014)
[31] S.M. Zhao, T.F. Feng, M.J. Zhang *et al.*, JHEP **02**, 130 (2020)
[32] M.E. Peskin and D.V. Schroeder, *An introduction to quantum field theory*, Addison Wesley: Reading U.S.A. (1995)
[33] G. Belanger, J.D. Silva, and H.M. Tran, Phys. Rev. D **95**, 115017 (2017)
[34] V. Barger, P.F. Perez, and S. Spinner, Phys. Rev. Lett. **102**, 181802 (2009)
[35] P.H. Chankowski, S. Pokorski, and J. Wagner, Eur. Phys. J. C **47**, 187 (2006)
[36] L.H. Su, S.M. Zhao, X.X. Dong *et al.*, Eur. Phys. J. C **81**, 433 (2021)
[37] T.F. Feng, L. Sun, and X.Y. Yang, Nucl. Phys. B **800**, 221-252 (2008)
[38] X.Y. Yang and T.F. Feng, Phys. Lett. B **675**, 43 (2009)
[39] CMS Collaboration, Phys. Lett. B **716**, 30 (2012)
[40] ATLAS Collaboration, Phys. Lett. B **716**, 1 (2012)
[41] Particle Data Collaboration, Review of Particle Physics, Prog. Theor. Exp. Phys. **2020**, 083C01 (2020)
[42] ATLAS Collaboration, Phys. Lett. B **796**, 68 (2019)
[43] G. Cacciapaglia, C. Csáki, G. Marandella *et al.*, Phys. Rev. D **74**, 033011 (2006)
[44] M. Carena, A. Daleo, B.A. Dobrescu *et al.*, Phys. Rev. D **70**, 093009 (2004)
[45] L. Basso, Adv. High Energy Phys. **2015**, 980687 (2015)
[46] T. Moroi, Phys. Rev. D **53**, 11 (1996)